LETTERS

El Niño in a changing climate

Sang-Wook Yeh[1], Jong-Seong Kug[1], Boris Dewitte[2], Min-Ho Kwon[3], Ben P. Kirtman[4] & Fei-Fei Jin[3]

El Niño events, characterized by anomalous warming in the eastern equatorial Pacific Ocean, have global climatic teleconnections and are the most dominant feature of cyclic climate variability on subdecadal timescales. Understanding changes in the frequency or characteristics of El Niño events in a changing climate is therefore of broad scientific and socioeconomic interest. Recent studies[1–5] show that the canonical El Niño has become less frequent and that a different kind of El Niño has become more common during the late twentieth century, in which warm sea surface temperatures (SSTs) in the central Pacific are flanked on the east and west by cooler SSTs. This type of El Niño, termed the central Pacific El Niño (CP-El Niño; also termed the dateline El Niño[2], El Niño Modoki[3] or warm pool El Niño[5]), differs from the canonical eastern Pacific El Niño (EP-El Niño) in both the location of maximum SST anomalies and tropical–midlatitude teleconnections. Here we show changes in the ratio of CP-El Niño to EP-El Niño under projected global warming scenarios from the Coupled Model Intercomparison Project phase 3 multi-model data set[6]. Using calculations based on historical El Niño indices, we find that projections of anthropogenic climate change are associated with an increased frequency of the CP-El Niño compared to the EP-El Niño. When restricted to the six climate models with the best representation of the twentieth-century ratio of CP-El Niño to EP-El Niño, the occurrence ratio of CP-El Niño/EP-El Niño is projected to increase as much as five times under global warming. The change is related to a flattening of the thermocline in the equatorial Pacific.

El Niño statistics exhibits variations on decadal timescales[7–10]. For instance, the properties of El Niño exhibited frequency and amplitude changes before and after the late 1970s[10]. During the late 1990s and 2000s, on the other hand, El Niño events show different characteristics in terms of location of maximum anomalous SST compared to the conventional El Niño[1–5]. For instance, a prolonged El Niño event during the period of 1990–1994, showed that, in the conventional El Niño region (the far eastern Pacific), the SST anomaly has waxed and waned, while the SST anomaly in the NINO4 region (160° E–150° W, 5° N–5° S) remained positive[1]. Other recent studies also argued that there exists a phenomenon in the tropical Pacific that is distinctly different from the canonical El Niño[11]—this variation[12] of El Niño has a 'horseshoe' spatial pattern, flanked by a colder SST on both sides along the Equator[2–5]. These studies led to various definitions of a new type of El Niño: the dateline El Niño[2], the El Niño Modoki[3], the central Pacific El Niño[4] and the warm pool El Niño[5]. The El Niño Modoki was named to represent the phenomenon in 2004 that had a maximum SST anomaly in the central tropical Pacific, differing from the conventional El Niño[3]. In addition, such modification in the structure of El Niño has implications for its teleconnection pattern in many countries surrounding the Pacific Ocean[2,13,14]. These observations raise the question of whether human-induced global warming[15] can modify our conventional view of El Niño.

We use the historical El Niño indices (the NINO3 SST index and the NINO4 SST index) and the Extended Reconstruction SST data for 1854–2007 to distinguish two variations of El Niño during the boreal winter (December-January-February, DJF). We term these the eastern Pacific El Niño (EP-El Niño) and the central Pacific El Niño (CP-El Niño). These terms have previously been used but with different definitions[4]. Here the terms EP-El Niño and CP-El Niño refer to the years in which the EP-El Niño and the CP-El Niño occurred during winter. Since the 1850s (Supplementary Table 1) the EP-El Niño occurred 32 times and the CP-El Niño occurred 7 times.

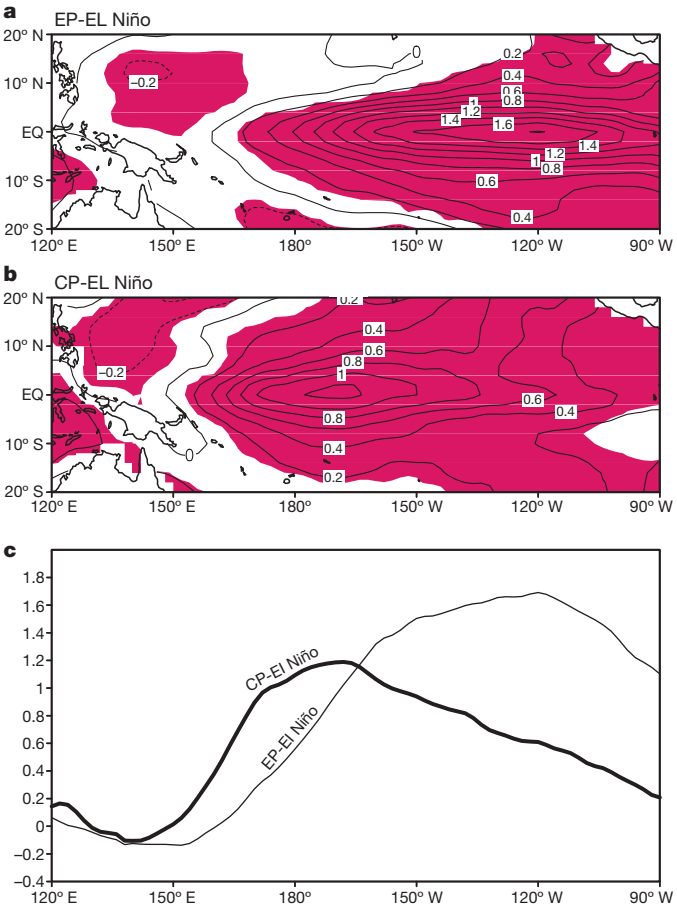

Figure 1 | Deviations of mean SST for the two characteristics of El Niño from the 1854–2006 climatology. **a**, The EP-El Niño; **b**, the CP-El Niño. The contour interval is 0.2 °C and shading denotes a statistical confidence at 95% confidence level based on a Student's *t*-test. **c**, The zonal structure for the composite EP-El Niño (thin line) and CP-El Niño (thick line) averaged over 2 °N to 2 °S.

[1]Climate Change and Coastal Disaster Research Department, Korea Ocean Research and Development Institute, 426-744, Ansan, Korea. [2]Laboratoire d'Etude en Geophysique et Oceanographie Spatiale, 14 avenue Edouard Belin, 31400, Toulouse, France. [3]Department of Meteorology, School of Ocean and Earth Science and Technology, University of Hawaii, 1680 East-West Road, Honolulu, 96822, Hawaii, USA. [4]University of Miami, Rosenstiel School of Marine and Atmospheric Science, 4600 Rickenbacker Causeway, Miami, Florida, 33149, USA.

Although the number of CP-El Niño events is relatively small, its frequency increased noticeably after 1990. For the period of 1854–2007, the occurrence ratio of the EP-El Niño before and after 1990 is 0.19 per year and 0.29 per year, respectively, whereas that of the CP-El Niño before and after 1990 is 0.01 per year and 0.29 per year, respectively. Simply put, this result indicates that anomalous warm SSTs in the central equatorial Pacific (that is, CP-El Niño) has been observed more frequently during recent decades[3]. This result is detectable even if the data are detrended (Supplementary Table 1) and taken from two additional SST data sets (Supplementary Table 3). A profound change in the characteristics of El Niño in recent years is also detectable in an 11-year window sliding correlation coefficients between the two NINO indices (Supplementary Fig. 1).

Figure 1a and b displays the deviation of mean SST for the EP-El Niño and the CP-El Niño from the climatological mean SST (1854–2006). As expected, the EP-El Niño (Fig. 1a) is characterized by maximum anomalous SST in the eastern equatorial Pacific; on the other hand, the centre of maximum SST in the CP-El Niño (Fig. 1b) is located near the dateline in the central equatorial Pacific. The SST composite in Fig. 1b is similar to the previously defined new type of El Niño[2–5] in spite of an extension of the analysed period and the use of the simple definition of the historical El Niño indices. Figure 1c clearly indicates that the centre of maximum SST of the CP-El Niño is significantly shifted to the west compared to that of the EP-El Niño. The details of the new type of El Niño suggested by previous studies[1–5] differ slightly from those of the CP-El Niño described here but the overall characteristics are similar.

The large difference of anomalous mean SST between the two types of El Niño results in changes in the total SST pattern in the tropical Pacific (not shown here), which determines the atmospheric response[16]. Figure 2a and b displays the composite rainfall corresponding to the EP-El Niño and the CP-El Niño. For the EP-El Niño (Fig. 2a), the centre of maximum anomalous rainfall is observed around the dateline; for the CP-El Niño (Fig. 2b) it is shifted westward to around 165° E. It is clear that anomalous rainfall is largely enhanced in the central and eastern equatorial Pacific and reduced in the western equatorial Pacific during the EP-El Niño compared to the CP-El Niño. Changes in the atmospheric diabatic forcing over the tropics have the potential to modify the tropical–midlatitude teleconnections to the El Niño[17,18]. Therefore, we would expect the midlatitude response to the EP-El Niño to differ from that of the CP-El Niño, and this has been shown to be true during the last 30 years[14]. This is evident from the patterns for anomalous mean atmospheric circulation at 500 hPa in the northern extratropics even over the extended period studied here (Fig. 2c and d) and anomalous mean SST and low-level winds (925 hPa) in the North Pacific (Fig. 2e and f) associated with both types of El Niño. The most striking difference in the teleconnection pattern between the two types of El Niño is in the position of the principal atmospheric centres of action in the extratropics (Fig. 2c and d). In addition, the anomalous North Pacific SST in response to the EP-El Niño and the CP-El Niño is also significantly different (Fig. 2e and f). The spatial manifestation of anomalous SST associated with the EP-El Niño (Fig. 2e) is characterized by cool temperatures in the central North Pacific with an elliptical shape and is accompanied by SST anomalies of the opposite sign to the east, north and south. In contrast to the EP-El Niño, anomalous easterly winds dominate over the central and eastern North Pacific, which may induce anomalous warm SSTs (Fig. 2f). The low-level winds during both types of El Niño are reasonably consistent with the wind–SST interactions in the midlatitudes[19].

Because El Niño and its teleconnections have dramatic societal impacts, such results call for an examination of the El Niño as simulated by the climate models under climate change projections. Here, we examine eleven coupled general circulation models (CGCMs): eleven control runs and eleven climate change runs (Supplementary Table 4). The control run is the twentieth-century climate change model simulation to year 2000 with anthropogenic and natural forcing (that is, 20C3M). The climate change run corresponds to

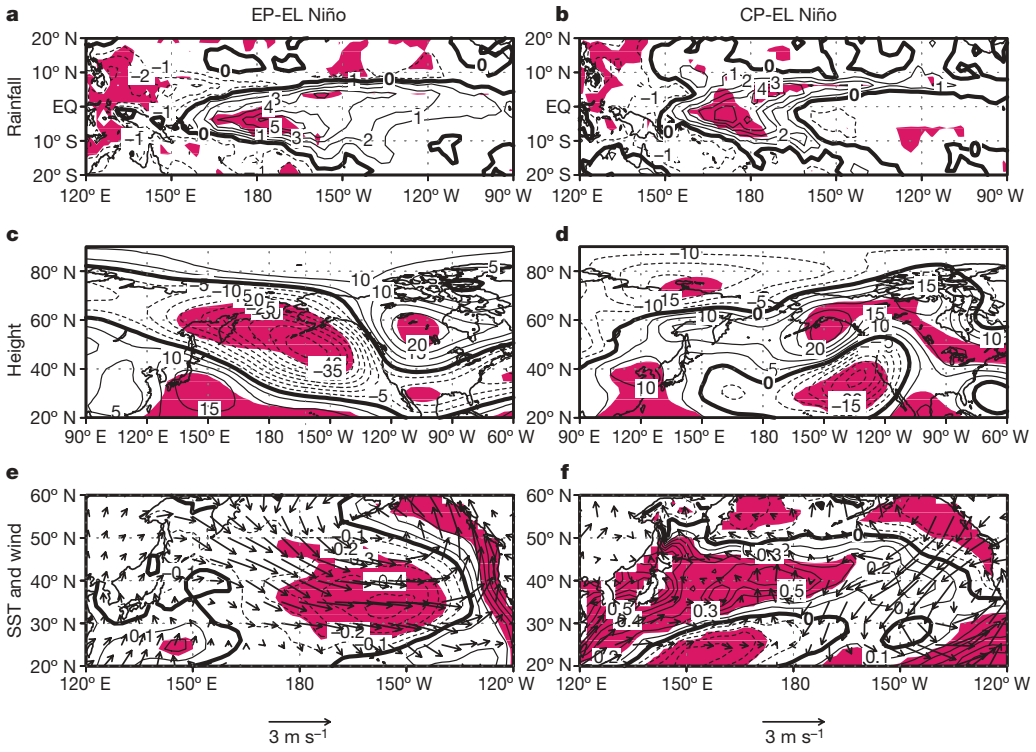

Figure 2 | Deviations for the two characteristics of El Niño from their climatology. **a**, **b**, The deviation of mean rainfall for the EP-El Niño (**a**) and the CP-El Niño (**b**). The contour interval is 1 mm per day. **c**, **d**, Mean geopotential height at 500 hPa. The contour interval is 5 m. **e**, **f**, Mean winds at 925 hPa (arrows, see scale arrow below) and mean SST (line). The solid (dotted) line denotes positive (negative) deviations from the mean. The contour interval is 0.1 °C. Shading in all panels indicates the region exceeding 95% significance based on a *t*-test and the zero line is denoted by the thick line. The climatology periods are 1979–2006 (for rainfall), 1950–2006 (for geopotential height and winds) and 1854–2006 (for SST), respectively.

the Special Report for Emission Scenario A1B climate change projection (that is, SRESA1B). Here, '20C3M run' refers to data from the 100-years simulation period for the 20C3M run. The term 'SRESA1B run' refers to the last 100 years of the SRESA1B run, in which the concentration of CO_2 is fixed to about 700 p.p.m. We show the ensemble mean composite of the EP-El Niño and the CP-El Niño in the 20C3M run and the SRESA1B run, respectively (Supplementary Figs 2 and 3).

Figure 3 displays the occurrence ratio of the CP-El Niño and EP-El Niño between the control run and the SRESA1B run. Despite the fact that there are discrepancies among CGCMs, it is remarkable that, in eight of 11 models, the occurrence ratio of the CP-El Niño versus the EP-El Niño increases from the 20C3M run to the SRESA1B run. The ensemble mean result for the eleven CGCMs is statistically significant at the 95% confidence level based on the bootstrap method. Furthermore, we test whether the ratio change in each CGCM is significant. The ratio of CP-El Niño to EP-El Niño significantly increases in four of 11 CGCMs at the 95% confidence level, and no other CGCMs show a significant decrease of the occurrence ratio of CP-El Niño to EP-El Niño. Statistical evidence for the increase of CP-El Niño under global warming becomes much stronger when we select the six CGCMs that most realistically capture the occurrence ratio of CP-El Niño to EP-El Niño in the 20C3M run compared to observations (see Supplementary Information). Thus, climate change projections indicate that the CP-El Niño occurs more frequently compared to the EP-El Niño. We also show how the SST variability changes from the 20C3M run to the SRESA1B run in the UKMO-HadCM3 model (Supplementary Fig. 4). We may hypothesize that more frequent CP-El Niño occurrence during recent decades is associated with an anthropogenic climate change. Such changes in El Niño characteristics in future climate are significant enough to modify the tropics–extratropics teleconnection pattern (Supplementary Fig. 5) despite the ability of current models realistically to simulate teleconnections. Furthermore, we expect that such frequent CP-El Niño occurrence under global warming could lead to more effective forcing of drought over India[3,13,20] and Australia[21].

Because El Niño dynamics is tightly linked to equatorial ocean mean state[22], we argue that such frequent CP-El Niño occurrence is associated with change in the background state under anthropogenic

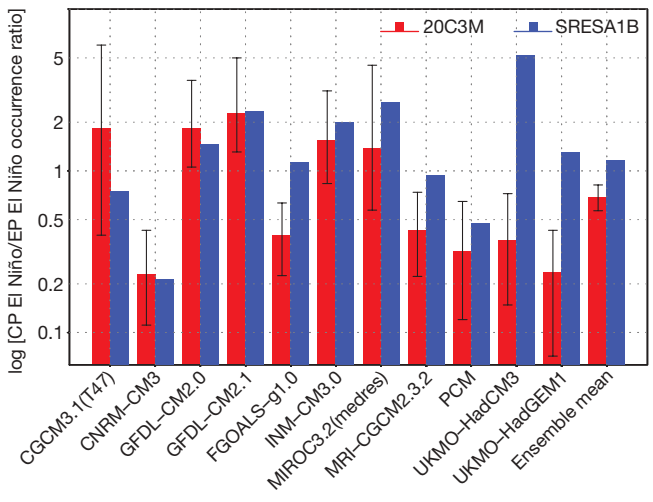

Figure 3 | The CP-El Niño/EP-El Niño occurrence ratio. Red bars, the 20C3M run; blue bars, the SRESA1B run. The vertical error bars denote the upper and lower limits associated with an increase and decrease of the CP-El Niño/EP-El Niño occurrence ratio at the 95% confidence level in the 20C3M run, respectively, based on a bootstrap method. Therefore, there is a significant increase (decrease) of the ratio of the CP-El Niño to the EP-El Niño from the 20C3M run to the SRESA1B run when the blue bar is above (below) the upper (lower) limit of the vertical segment. The *y*-axis scale is a common logarithmic scale.

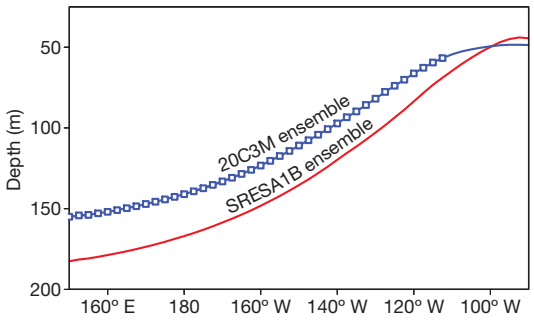

Figure 4 | The ensemble mean thermocline depth. The red line denotes the 20C3M ensemble and the blue line denotes the SRESA1B run in the nine CGCMs: theCGCM3.1(T47), the CNRM-CM3, the GFDL-CM2.0, the GFDL-CM2.1, the FGOALS-g1.0, the MIROC3.2(medres), the MRI-CGCM2.3.2, the PCM and the UKMO-HadCM3. In both runs, the thermocline depth is defined as the depth of the isotherm of the averaged value of temperatures where the vertical gradient of temperature is a maximum along the Equator. The blue data points indicate that the change in the mean thermocline depth from the 20C3M run to the SRESA1B run is significant at the 95% confidence level, based on a *t*-test.

global warming, in particular change in the thermocline structure in the equatorial Pacific. Figure 4 displays the change in mean thermocline depth from the control run to the SRESA1B run. The mean thermocline has risen under global warming in the western-central Pacific, whereas it is slightly deeper in the far eastern Pacific. This results in an overall flattening of the equatorial mean thermocline, which is consistent with a weakened atmospheric Walker circulation and trade winds under global warming[23] and even changes in the thermocline depth during recent decades[3]. In other words, the SST warms as a result of thermal forcing, which leads to weaker easterlies and enhanced poleward Sverdrup transport and hence a shoaling of the thermocline depth. How might this affect the stability of the CP-El Niño?

We can understand this destabilizing process in terms of the two important feedback processes associated with El Niño dynamics, that is, thermocline feedback versus zonal advective feedback. Although the trade winds reduce under global warming, this reduces upwelling and thus the thermocline feedback. In contrast, a shallower thermocline in the central Pacific, as in the SRESA1B run, tends to enhance the SST anomaly induced by vertical advection there (because isotherm vertical displacements within the thermocline depth can more easily influence the SST). In addition, such a shallowing thermocline tends to dominate the zonal advective feedback in the central Pacific, which may promote a more intense CP-El Niño[5,22,24]. Overall, the change in thermocline structure from the 20CM3 run to the SRESA1B run is consistent with the increased variability of the SST anomaly in the central Pacific. This physical consistency fits with the result reported here: the probable increased occurrence of the CP-El Niño under global warming.

METHODS SUMMARY

The two kinds of El Nino were diagnosed from observations and eleven models of the Program for Climate Model Diagnosis and Intercomparison (PCMDI). We propose a classification based on the historical NINO3 and NINO4 SST indices during winter and inferred from composite analyses to distinguish the CP-El Niño from the EP-El Niño. Applied to the simulation for the present (20C3M) and for the future (SRESA1B), we derived a projection of the occurrence ratio of CP-El Niño to EP-El Niño. See the Supplementary Information.

Full Methods and any associated references are available in the online version of the paper at www.nature.com/nature.

Received 29 December 2008; accepted 21 July 2009.

1. Latif, M., Kleeman, R. & Eckert, C. Greenhouse warming, decadal variability, or El Niño? An attempt to understand the anomalous 1990s. *J. Clim.* **10**, 2221–2239 (1997).

2. Larkin, N. K. & Harrison, D. E. Global seasonal temperature and precipitation anomalies during El Niño autumn and winter. *Geophys. Res. Lett.* **32,** L13705, doi:10.1029/2005GL022738 (2005).
3. Ashok, K., Behera, S. K., Rao, S. A., Weng, H. & Yamagata, T. El Niño Modoki and its possible teleconnection. *J. Geophys. Res.* **112,** C11007, doi:10.1029/2006JC003798 (2007).
4. Kao, H.-Y. & Yu, J.-Y. Contrasting Eastern-Pacific and Central-Pacific types of ENSO. *J. Clim.* **22,** 615–632 (2009).
5. Kug, J.-S., Jin, F.-F. & An, S.-I. Two types of El Niño events: cold tongue El Niño and warm pool El Niño. *J. Clim.* **22,** 1499–1515 (2009).
6. Meehl, G. A. *et al.* The WCRP CMIP3 multimodel dataset. *Bull. Am. Meteorol. Soc.* **88,** 1383–1394 (2007).
7. Trenberth, K. & Shea, D. J. On the evolution of the Southern Oscillation. *Mon. Weath. Rev.* **115,** 3078–3096 (1987).
8. Cobb, K., Charles, C., Cheng, H. & Edwards, R. El Niño/Southern Oscillation and tropical Pacific climate during the last millennium. *Nature* **424,** 272–276 (2003).
9. An, S.-I. & Jin, F.-F. Nonlinearity and asymmetry of ENSO. *J. Clim.* **17,** 2399–2412 (2004).
10. An, S.-I. & Wang, B. Interdecadal change of the structure of the ENSO mode and its impact on the ENSO frequency. *J. Clim.* **13,** 2044–2055 (2000).
11. Rasmusson, E. M. & Carpenter, T. H. Variations in tropical sea surface temperature and surface wind fields associated with the southern oscillation/El Niño. *Mon. Weath. Rev.* **110,** 354–384 (1982).
12. Trenberth, K. E. & Stepaniak, D. P. Indices of El Nino evolution. *J. Clim.* **14,** 1697–1701 (2001).
13. Weng, H., Ashok, K., Behera, S. K., Rao, S. A. & Yamagata, T. Impacts of recent El Nino Modoki on dry/wet conditions in the Pacific Rim during boreal summer. *Clim. Dyn.* **29,** 113–129 (2007).
14. Weng, H., Behera, S. K. & Yamagata, T. Anomalous winter climate conditions in the Pacific Rim during recent El Niño Modoki and El Niño events. *Clim. Dyn.* **32,** 663–674 (2009).
15. Solomon, S, *et al.* (eds) *Climate Change 2007: The Physical Science Basis* (Cambridge University Press for the Intergovernmental Panel on Climate Change, 2007).
16. Hoerling, M. P. & Kumar, A. Atmospheric response patterns associated with tropical forcing. *J. Clim.* **15,** 2184–2203 (2002).
17. Alexander, M. *et al.* The atmospheric bridge: The influence of ENSO teleconnections on air-sea interaction over the global oceans. *J. Clim.* **15,** 2205–2228 (2002).
18. Barsugli, J. & Sardeshmukh, P. D. Global atmospheric sensitivity to tropical SST anomalies throughout the Indo-Pacific basin. *J. Clim.* **15,** 3427–3442 (2002).
19. Cayan, D. R. Latent and sensible heat flux anomalies over the northern oceans: driving the sea surface temperature. *J. Phys. Oceanogr.* **22,** 859–881 (1992).
20. Kumar, K. K., Rajagopalan, B., Hoerling, M., Bates, G. & Cane, M. Unraveling the mystery of Indian monsoon failure during El Niño events. *Science* **314,** 115–119 (2006).
21. Wang, G. & Hendon, H. H. Sensitivity of Australian rainfall to inter-El Nino variations. *J. Clim.* **20,** 4211–4226 (2007).
22. Fedorov, A. V. & Philander, S. G. H. Is El Niño changing? *Science* **288,** 1997–2002 (2000).
23. Vecchi, G. A. *et al.* Weakening of tropical Pacific atmospheric circulation due to anthropogenic forcing. *Nature* **441,** 73–76 (2006).
24. Bejarano, L. & Jin, F.-F. Coexistence of equatorial coupled mode of ENSO. *J. Clim.* **21,** 3051–3067 (2008).

Supplementary Information is linked to the online version of the paper at www.nature.com/nature.

Acknowledgements We acknowledge the international modelling groups for providing their data and PCMDI and the IPCC Data Archive at LLNL/DOE for collecting, archiving and making the data readily available. S.-W.Y. and J.-S.K. are supported by KORDI (grants PE98401, PP00720). B.D. benefited from funding from the PCCC project (Peru Chile Climate Change) of the ANR (Agence Nationale de la Recherche). J.-S. K. and F.-F. J. are also supported by NSF grants ATM 060552 and AMT 065145 and NOAA grant GC01-229.

Author Contributions S.-W.Y., M.K. and J.-S.K. contributed to analysis. S.-W.Y., J.-S.K., B.D, B.P.K. and F.-F.J. contributed to writing the paper. All authors discussed the results and commented on the manuscript.

Author Information Reprints and permissions information is available at www.nature.com/reprints. Correspondence and requests for materials should be addressed to S.-W.Y. (swyeh@kordi.re.kr).

METHODS

The SSTs analysed in this study are taken from the Extended Reconstruction SST version 2 (ERSST.v2) covering the period of 1854–2007 released by the National Climatic Data Center[25]. In addition, the Climate Prediction Center (CPC) Merged Analysis of Precipitation (CMAP) data are used for the period of 1979–2007 (ref. 26). Atmospheric circulation data were taken from the National Centers for Environmental Prediction/National Center for Atmospheric Science (NCEP/NCAR) reanalysis data[27] which use a grid with a horizontal resolution of $2.5^\circ \times 2.5^\circ$. To define the two types of El Niño we first collect the years in which the NINO3 SST index during the boreal winter (DJF) is above 0.5 °C or the NINO4 SST index during winter is above 0.5 °C. The DJF NINO3 SST index is defined by the time series of the seasonal (that is, DJF) mean SST anomaly averaged over the NINO3 region (150° W–90° W, 5° N–5° S). Similarly, the DJF NINO4 SST index is the same as the DJF NINO3 SST index except for the NINO4 region (160° E–150° W, 5° N–5° S). The seasonal mean SST anomaly is defined as seasonal mean deviations from a climatological (1854–2006) seasonal mean SST. Of those years, an EP-El Niño year is defined as a year in which the DJF NINO3 SST index is greater than the DJF NINO4 SST index. On the other hand, a CP-El Niño year is defined as a year in which the DJF NINO4 SST index is greater than the DJF NINO3 SST index. Using this classification, the composite for mean precipitation, 500 hPa geopotential height and surface winds is derived for the two types of El Niño. The seasonal mean anomalies for these variables are also defined as seasonal mean deviations from a climatological seasonal mean.

The method is further applied to eleven CGCM simulations in the 20C3M run and the SRESA1B run made by the Program for Climate Model Diagnosis and Intercomparison (PCMDI). The occurrence ratio of CP-El Niño to EP-El Niño is derived and the change in statistics of this parameter from the 20C3M run to the SRESA1B run is examined. To examine whether the change in the CP-El Niño/EP-El Niño occurrence ratio from the SREA1B run is significantly different from the internal variability of the 20C3M run, we constructed the probability distribution function of the internal variability for the occurrence ratio from each individual model in the 20C3M run using a bootstrap method[28]. First, we randomly select N El Niño events of the total El Niño events for each model in the 20C3M run. During the random selection process, overlapping selection is allowed, so that one El Niño event can be selected again. Note that N is a total number of the CP-El Niño and EP-El Niño events simulated from an individual model; therefore, N differs for each model. From the selected N events in each model, we separate them into the CP-El Niño and EP-El Niño events and then we calculate CP-El Niño/EP-El Niño occurrence ratio. By repeating this process 10,000 times, we obtain 10,000 values for the occurrence ratio and the probability distribution function for the occurrence ratio is constructed for each model. The top and bottom of each error bar in Fig. 3 represents the 2.5% and 97.5% ranking from the probability distribution function, respectively, indicating the 95% confidence level. If the occurrence ratio from the SREA1B run is out of the range of the 2.5% and 97.5% ranking, it indicates that the change in occurrence ratio from the 20C3M run to the SRESA1B run is significant at the 95% confidence level.

25. Smith, T. M. & Reynolds, R. W. Improved extended reconstruction of SST (1854–1997). *J. Clim.* **17,** 2466–2477 (2004).
26. Xie, P., &. Arkin, P. A. Global precipitation: a 17-year monthly analysis based on gauge observations, satellite estimates, and numerical outputs. *Bull. Am. Meteorol. Soc.* **78,** 2539–2558 (1997).
27. Kalnay, E. *et al.* The NCEP/NCAR 40-year reanalysis project. *Bull. Am. Meteorol. Soc.* **77,** 437–471 (1996).
28. Efron, B. *The Jackknife, the Bootstrap, and Other Resampling Plans* 1–92 (Society for Industrial and Applied Mathematics, 1982).

ERRATUM

doi:10.1038/nature08546

El Niño in a changing climate

Sang-Wook Yeh, Jong-Seong Kug, Boris Dewitte, Min-Ho Kwon, Ben P. Kirtman & Fei-Fei Jin

Nature **461**, 511–514 (2009)

In Figure 4 of this letter, the key for the 20C3M ensemble (red line) and the SRESA1B ensemble (blue line) were inadvertently mislabelled. The correct figure is shown below.